Journal of Power Sources 185 (2008) 272–279

Contents lists available at ScienceDirect

Journal of Power Sources

journal homepage: www.elsevier.com/locate/jpowsour

Polymer electrolyte membrane fuel cell contamination: Testing and diagnosis of toluene-induced cathode degradation

Hui Li[a], Jianlu Zhang[a], Khalid Fatih[a], Zhenwei Wang[a], Yanghua Tang[a], Zheng Shi[a], Shaohong Wu[a], Datong Song[a], Jiujun Zhang[a,*], Nengyou Jia[b], Silvia Wessel[b], Rami Abouatallah[c], Nathan Joos[c]

[a] *Institute for Fuel Cell Innovation, National Research Council Canada, Vancouver, BC V6T 1W5, Canada*
[b] *Ballard Power Systems, Inc., Burnaby, BC V5J 5J8, Canada*
[c] *Hydrogenics Corp., Mississauga, ON L5R 1B8, Canada*

ARTICLE INFO

Article history:
Received 26 May 2008
Received in revised form 4 July 2008
Accepted 4 July 2008
Available online 17 July 2008

Keywords:
PEM fuel cells
Air impurity
Toluene contamination
Electrode kinetics
Mass transfer

ABSTRACT

The effects of toluene contamination on the performance of polymer electrolyte membrane (PEM) fuel cells were investigated, using various levels of toluene concentration in the air streams, under different operational conditions and with different catalyst loadings. Constant-current polarization and electrochemical impedance spectroscopy (EIS) were conducted to analyze the poisoning behaviour of toluene. The severity of the contamination effect increased with an increase in both the current density and the toluene concentration, but decreased with an increase in both the relative humidity (RH) and the cathode-side Pt loading. The toluene-poisoned fuel cell could not be fully recovered by replacing toluene-contaminated air with pure air. EIS measurements revealed that both kinetic resistance and mass transfer resistance increased as a result of toluene contamination, while membrane resistance remained unchanged. However, the increase in kinetic resistance was a major contributor to cell performance degradation.
Crown Copyright © 2008 Published by Elsevier B.V. All rights reserved.

1. Introduction

The PEM fuel cell is considered a promising energy converter due to its high power density, high efficiency, and low/zero emissions. However, significant challenges still exist in the areas of development and application, particularly issues of reliability/durability and cost. These two major challenges are both associated with degradation in fuel cell performance. Contamination caused by fuel and/or oxidant impurities is one identified factor that contributes considerably to fuel cell degradation [1,2].

In the past several years, extensive research has been carried out on contamination by fuel-side impurities, including CO, H_2S, NH_3, and hydrocarbons. CO [3–6] and H_2S [7–9] in particular have attracted attention, due to their inevitable presence in hydrogen-rich reformate gas. However, the literature contains much less information on the effects of contamination by air-side (i.e., oxidant-side) impurities. Due to air pollution induced by emissions from automotive and other manufacturing industries, a considerable quantity of pollutants such as NO_x ($NO + NO_2$), SO_x ($SO_2 + SO_3$), CO_x ($CO + CO_2$), as well as volatile organic compounds (VOCs) are present in the atmosphere, any of which will contaminate the fuel cell catalyst layers and degrade performance if a fuel cell is operated with air as the oxidant [3]. Therefore, efforts must be made to overcome contamination problems and develop mitigation strategies, in order to improve the environmental adaptability of the fuel cell system [10,11].

The effects of the air-side impurities NO_x, SO_x, and CO_x on fuel cell performance have been studied recently by several researchers [11–13]. With respect to VOCs, including benzene, toluene, and ethylene, only one publication to date has briefly reported on the contamination effect of benzene present in a battlefield environment [11]. VOCs are present in the atmosphere as a result of decorative materials and dry cleaning solvents (in indoor environments), or of industrial, agricultural, and biological processes (in outdoor environments). It has been reported that benzene has a significant contamination effect on fuel cell performance. For example, with 50 ppm benzene in the air, the cell voltage can drop by 160 mV within 15 min at 0.2 A cm^{-2}. It is expected that VOCs, even at low concentration levels, would cause significant cell performance loss. Therefore, conducting experimental investigations and gaining a fundamental understanding of the contamination effect of VOCs on fuel cell performance are necessary activities for developing practical PEM fuel cell applications.

In this study, toluene was selected as a typical VOC to observe fuel cell contamination. To our knowledge, the effect of toluene, as a VOC air contaminant, on PEM fuel cell performance has never been

* Corresponding author. Tel.: +1 604 221 3087.
E-mail address: jiujun.zhang@nrc-cnrc.gc.ca (J. Zhang).

0378-7753/$ – see front matter. Crown Copyright © 2008 Published by Elsevier B.V. All rights reserved.
doi:10.1016/j.jpowsour.2008.07.006

reported in the literature. It is known that VOCs such as benzene and toluene can adsorb onto metal surfaces to form 3-D structures [14,15], which may compete with the oxygen reduction reaction (ORR) for catalytic sites at the cathode side of an operational PEM fuel cell. It is also known that toluene can be electrochemically oxidized at the Pt surface, forming intermediate species or carbon oxides that could poison the cathode catalyst [15]. In addition, toluene adsorbs on the surface of the catalyst carbon support, which might modify the surface properties of the PEM fuel cell catalyst layers. Furthermore, toluene could also adsorb on the surface of the gas diffusion layer (GDL), potentially causing a change in the GDL surface properties.

This work is part of our ongoing effort to fundamentally understand the effect of toluene contamination on fuel cell performance, an undertaking that includes contamination testing, empirical and theoretical model development, as well as electrochemical study. In this study, toluene contamination tests at different toluene concentrations and under different operational conditions were carried out, and diagnostic investigation of fuel cell performance degradation was conducted, to gain insights into the contamination mechanism of toluene.

2. Experimental

2.1. Set-up of the toluene–air mixing system

The configuration of the contaminant mixing system is illustrated in Fig. 1. Toluene from a toluene–air cylinder is introduced through a mass flow controller (MFC) into a heated mixer, which is a 1.0 m-long coil made of stainless steel tubing (diam. 0.25 in.). To prevent gas backflow, two check valves (CVs) are installed: one downstream from the humidifier and the other downstream from the MFC of the toluene-contaminated air. The toluene concentration in the mixer is controlled by changing the ratio between the flow rate of pure air and that of toluene-contaminated air. The dew point of the humidifier is calculated and controlled by taking into consideration the diluting effect of the dry toluene-contaminated air, which maintains the relative humidity (RH) of the air mixture in the fuel cell at the desired level.

To avoid other potential impurities, certified toluene–air (2–50 ppm from Linde Canada) and highly purified air (99.99% from Praxair Canada) were used throughout all tests. The mixing system was validated by analysis of the gas samples collected at the fuel cell inlet. The maximum and minimum deliverable toluene concentrations were controlled according to the concentration of toluene in the toluene–air cylinder, the oxygen stoichiometric number, and the current density.

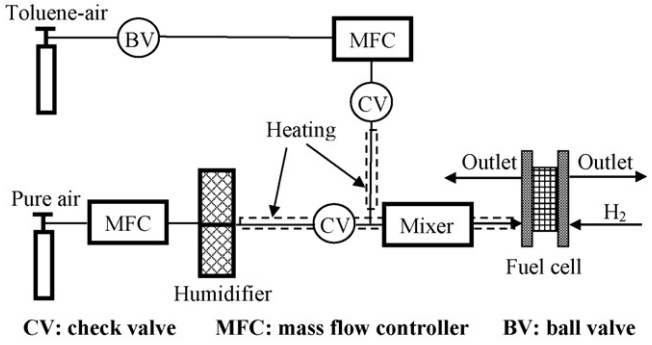

Fig. 1. System set-up for the effect of toluene contamination on fuel cell performance.

Table 1
Operating conditions for the contamination tests

Name of tests	Concentration screening	Effect of RH	Effect of cathode Pt loading
Stoichiometry, H_2/air	1.5/3.0	1.5/3.0	1.5/3.0
Cell temperature, °C	80	80	80
Back pressure, psig	30	30	30
Current density, A cm^{-2}	0.0, 0.2, 0.5, 0.75, 1.0	1.0	1.0
Toluene conc., ppm	1, 5, 10, 50	5	5
Pt loading, mg cm^{-2}	0.4	0.4	0.2, 0.4, 0.6
RH, %	80	20, 50, 80, 100	80
Total number of tests	20	4	3

2.2. MEA and fuel cell testing

The membrane electrode assembly (MEA), with an active area of 50 cm^2, consisted of SGL GDLs with 20% PTFE, and a catalyst coated membrane (CCM) made of Nafion® 211 membrane (Ion Power, Inc.). The anode-side Pt loading was 0.4 mg cm^{-2} for all tests, and the cathode-side Pt loadings were 0.2, 0.4, and 0.6 mg cm^{-2} in different tests. A fresh MEA was employed for each contamination test.

Single-cell hardware with end plates, heating cartridges, and a temperature controller was purchased from Teledyne (50 cm^2 CH-50). The flow-field plates were designed and fabricated in-house using single serpentine flow channels with 1.2 mm width, 1.0 mm channel depth, and 1.0 mm landing. A Fideris 100 W fuel cell test station was employed for all tests.

In all fuel cell tests, both with and without toluene present, the voltage–current polarization curves (steady-state polarization curves) were collected using a load bank controlled in a constant-current pattern. For the contamination tests, three sets of tests were carried out: (1) concentration screening, in which contamination tests were conducted for four toluene contamination levels (1, 5, 10, and 50 ppm vol/vol), each under five current densities (0.0, 0.2, 0.5, 0.75, and 1.0 A cm^{-2}); (2) the effect of RH on toluene contamination, which was performed for four levels of RH (20, 50, 80, and 100%) and 5 ppm toluene in the air stream; (3) the effect of the cathode Pt loading on toluene contamination, which included contamination tests with three different cathode Pt loadings (0.2, 0.4, and 0.6 mg cm^{-2}). Operating conditions for the three sets of contamination tests were: cell temperature, 80 °C; back pressure, 30 psig; and H_2/air stoichiometries, 1.5/3.0. Other conditions are listed in Table 1. For each contamination test, AC impedance measurements were performed both prior to the introduction of toluene and at the end of the contamination duration, to evaluate the change in cell resistances caused by toluene contamination. The impedance spectra were recorded with a Solartron 1252 Frequency Response Analyzer (FRA) by sweeping frequencies over the range of 10 kHz to 0.1 Hz.

3. Results and discussion

3.1. Concentration screening

3.1.1. Effects of toluene concentration at various current densities

The purpose of this set of tests was to investigate the impact of various levels of toluene on cell performance under different current densities. The curves of cell voltage vs. time for various contamination levels of toluene at current densities of 0.2, 0.5, 0.75, and 1.0 A cm^{-2} are shown in Fig. 2. It can be seen that at all current densities, the cell voltage starts to decline immediately after the toluene is introduced into the air, and then reaches a plateau. These plateau voltages indicate the saturated nature of the toluene contamination. For example, the cell voltage drops from 0.645 to 0.522 V at 1.0 A cm^{-2} within 30 min of the cathode being contin-

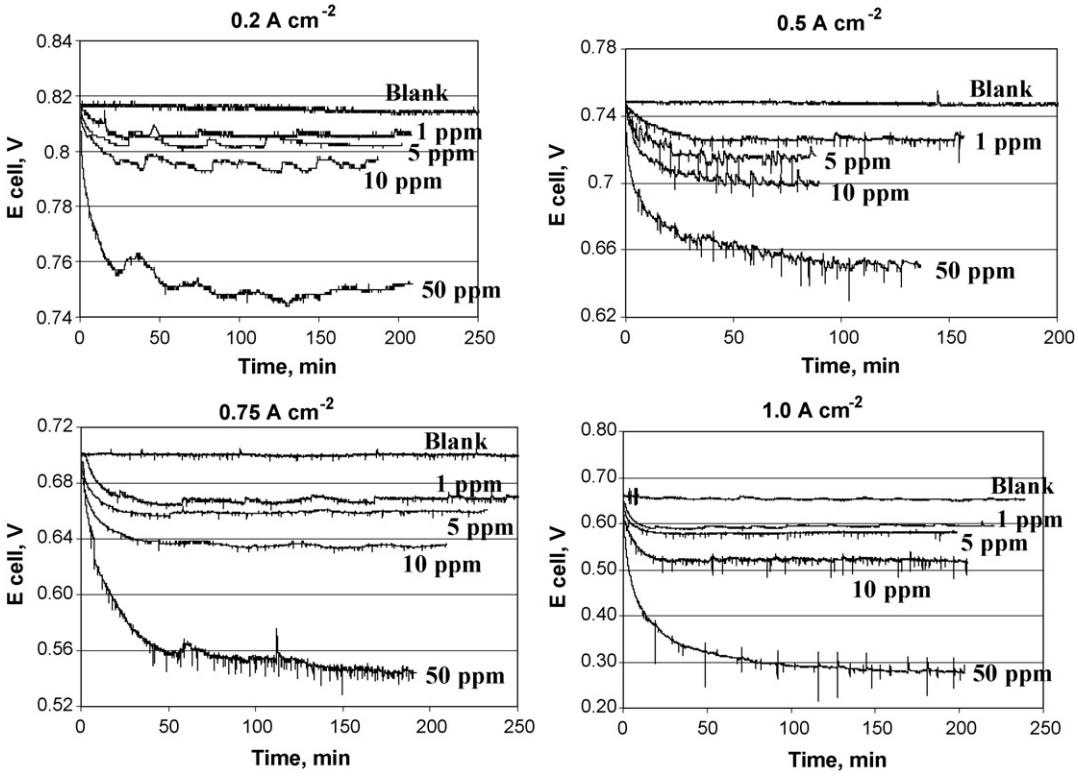

Fig. 2. Voltage–time curves with various levels of toluene at different-current densities. Operating conditions: stoichiometry: 1.5/3.0 for H_2/air; RH: 80%; cell temperature: 80 °C; backpressure: 30 psig. Anode/cathode Pt loading: 0.4 mg cm^{-2}.

uously exposed to 10 ppm toluene, and then begins to level off. The spikes in cell voltage on the curves are related to the issue of catalyst layer water management, induced by toluene contamination. In the absence of toluene, no obvious spikes are observed on the voltage–time curves, demonstrating that toluene contamination could indeed cause difficulties with respect to water removal (or water flooding [16]) in the catalyst layer. This will be further discussed in a later section of this paper.

Contamination tests at open circuit voltage (OCV) with various levels of toluene concentration demonstrate a different trend from values obtained with electric loads (or with current densities). It can be observed from Fig. 3 that a fuel cell running at OCV without the presence of toluene deteriorates steadily, i.e., showing a cell voltage drop of about 110 mV within 26 h. This is in agreement with what has been reported in literature [17]. In the presence of 1, 5, 10, and 50 ppm toluene, the degradation rates at OCV are not significantly different from the rate without toluene contamination. Therefore, it can be concluded that toluene in the air stream has an insignificant effect on OCV within the toluene concentration range tested in this study (0–50 ppm). In our recent study of the adsorption and reaction behaviour of toluene on the Pt cathode [18], using cyclic voltammetry (CV) and rotating disc electrode (RDE) methodologies, we observed that the toluene begins to be oxidized to carbon dioxide at a potential of about 0.8 V at 80 °C. This could explain why toluene does not have a significant contamination effect on cell performance when operated at OCV (Fig. 3), where the cell voltage is about 0.96 V and all the adsorbed toluene at the catalyst surface would probably be oxidized.

Table 2 summarizes steady-state cell voltage drop as a function of current density at different toluene concentrations, and Fig. 4 illustrates steady-state polarization curves as they are affected by various levels of toluene contamination. A general observation from Table 2 and Fig. 4 is that the magnitude of the negative impact of toluene on cell performance increases as both toluene concentration and current density increase. Specifically, as toluene concentration increases, (1) the cell voltage drop becomes larger at the same current density, (2) the steady-state polarization curve becomes non-parallel with the baseline polarization curve (without toluene), and (3) the cell voltage starts to experience a sudden drop in the high current density region. These observations can be semi-quantitatively understood through the following discussion.

If the anode polarization is negligible and the cathode polarization is in the Tafel region, a fuel cell voltage can be expressed as Eq. (1) [19]:

$$V_{\text{cell}} = E^{\text{OCV}} + b\left[\ln(i^{\text{o}}_{\text{O}_2}) - \ln\left(\frac{I_{\text{cell}}I_{\text{dc}}}{I_{\text{dc}} - I_{\text{cell}}}\right)\right] - I_{\text{cell}}R_{\text{m}} \quad (1)$$

where V_{cell} is the cell voltage, E^{OCV} is the open circuit voltage, b is the Tafel slope, $i^{\text{o}}_{\text{O}_2}$ is the apparent exchange current density for the cathode O_2 reduction reaction, I_{dc} is the diffusion limiting current density for the ORR, I_{cell} is the fuel cell current density, and R_{m} is the membrane resistance.

When toluene is present in the air stream, adsorbed toluene on the Pt surface occupies the catalyst sites that would otherwise be available for the ORR, thus reducing the apparent exchange current density of the ORR on the Pt catalyst from $i^{\text{o}}_{\text{O}_2}$ to $i^{\text{o}}_{\text{O}_2}(1-\theta_{\text{T}})$, where θ_{T} is the surface coverage of toluene on the catalyst. According to our work, the Langmuir adsorption model is valid for toluene adsorption on a Pt surface, therefore θ_{T} can be expressed as [15]:

$$\frac{1}{\theta_{\text{T}}} = \frac{1}{C_{\text{T}}B_{\text{ads}}} + 1 \quad (2)$$

in which B_{ads} is a parameter reflecting the affinity of toluene for the Pt surface, and C_{T} is the bulk concentration of toluene. Apparently, θ_{T} can be increased by increasing the toluene concentration. Taking into consideration the presence of toluene, Eq. (1) becomes

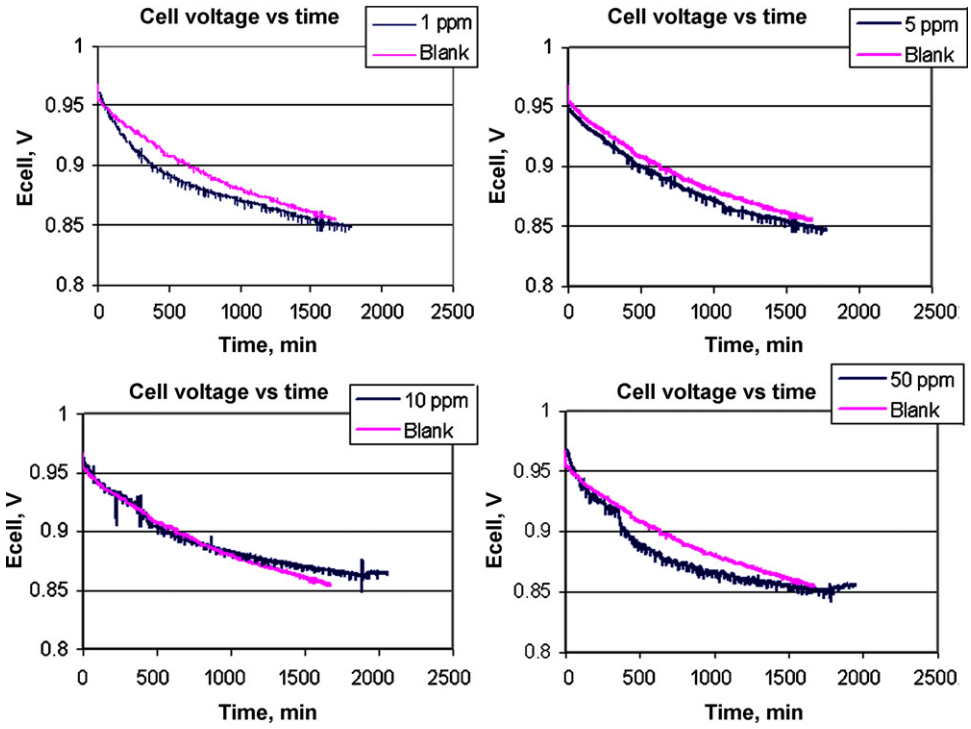

Fig. 3. Voltage–time curves at open circuit voltage with 1, 5, 10, and 50 ppm toluene, respectively. The curves in the absence of toluene were used for comparison. Operating conditions: stoichiometry: 1.5/3.0 for H_2/air; RH: 80%; cell temperature: 80 °C; backpressure: 30 psig. MEA: anode/cathode Pt loading: 0.4 mg cm^{-2}.

Table 2
Summary of the cell voltage drops as functions of toluene concentration and current density

Toluene concentration, ppm	Cell voltage drops at various current densities, mV				
	OCV	0.2 A cm^{-2}	0.25 A cm^{-2}	0.75 A cm^{-2}	1.0 A cm^{-2}
1	0	12	22	33	56
5	0	17	30	40	72
10	0	39	50	68	132
50	0	69	100	151	371

Operating conditions are the same as given for Fig. 2.

Eq. (3):

$$V_{\text{cell}} = E^{\text{OCV}} + b\left[\ln(i^{\text{o}}_{\text{O}_2}) + \ln(1-\theta_{\text{T}}) - \ln\left(\frac{I_{\text{cell}}I_{\text{dc}}}{I_{\text{dc}}-I_{\text{cell}}}\right)\right] - I_{\text{cell}}R_{\text{m}} \quad (3)$$

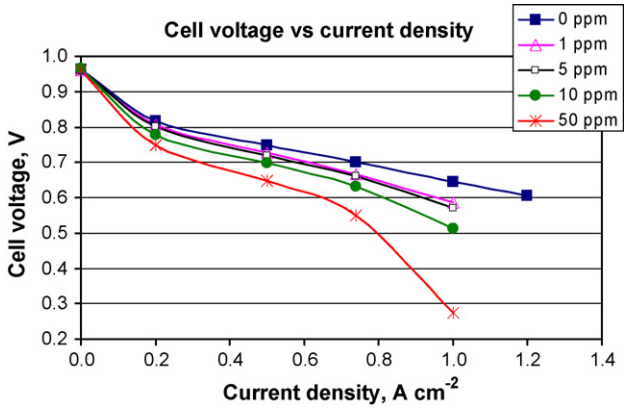

Fig. 4. Steady-state polarization curves of a fuel cell contaminated by toluene in the air stream. Operating conditions: stoichiometry: 1.5/3.0 for H_2/air; RH: 80%; cell temperature: 80 °C; backpressure: 30 psig. MEA: anode/cathode Pt loading: 0.4 mg cm^{-2}.

Eq. (3) demonstrates that as toluene concentration increases, the toluene coverage on the catalyst surface θ_{T} increases, which drives the cell voltage to drop even more. In addition, the presence of toluene increases the value of the Tafel slope b of the ORR, as reported in our work [18], which explains the non-parallel feature or the increasing degradation behaviour of the polarization curves caused by toluene contamination. Lastly, as toluene concentration increases, the fuel cell starts to experience more serious water management issues, as indicated by the negative spikes in the cell voltage seen in Fig. 2, thus decreasing the diffusion limiting current density I_{dc}. As a result, when the current density increases to some extent, the fuel cell begins to run nearly at diffusion limiting current density, which results in a sudden increase in the term $\ln(I_{\text{cell}}I_{\text{dc}}/I_{\text{dc}}-I_{\text{cell}})$ of Eq. (3), and thus a corresponding sudden drop in V_{cell}.

3.1.2. *Measurements using electrochemical impedance spectroscopy (EIS)*

Fig. 5 shows a representative set of Nyquist plots that were obtained during the contamination test with 5 ppm of toluene at 1.0 A cm^{-2}. The high-frequency intercept with the real impedance axis of the Nyquist plot represents the membrane resistance, and the two semicircles correspond to the charge transfer (kinetic) resistance (first semicircle) and mass transfer resistance (second

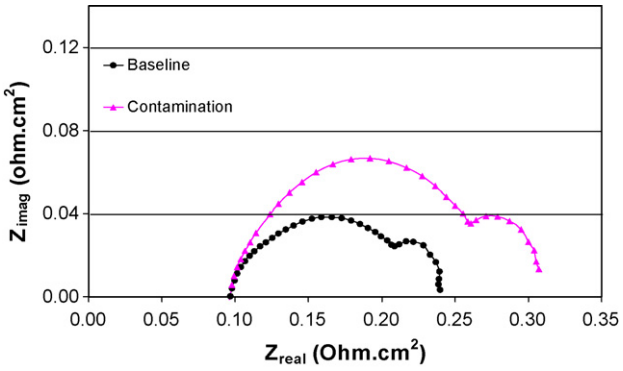

Fig. 5. Nyquist plots measured before toluene injection and at the end of toluene contamination. Operating conditions: toluene concentration: 5 ppm; current density: 1.0 A cm^{-2}; stoichiometry: 1.5/3.0 for H_2/air; RH: 80%; cell temperature: 80 °C; backpressure: 30 psig. MEA: anode/cathode Pt loading: 0.4 mg cm^{-2}.

semicircle) [20]. Clearly, in the case of Fig. 5, the kinetic and mass transfer resistances are significantly increased as a result of toluene contamination, while the membrane resistance remains unchanged. To determine which individual resistance among the three (membrane, kinetic, and mass transfer) is most responsible for performance degradation is of great importance for understanding the mechanism of toluene contamination. Therefore, all the EIS measurement data collected during the toluene contamination tests were fitted to obtain numerical data on the three individual resistances, according to the equivalent circuit shown in Fig. 6. R_m is the high-frequency resistance (the intercept on the Z_{real} axis at the high-frequency end), which represents the membrane resistance; R_c is the charge transfer resistance, dominated by the oxygen reduction reaction; CPE_1 (constant phase element) represents the R_c associated catalyst layer capacitance properties; R_{mt} is the resistance related to the mass transfer of O_2 in both the

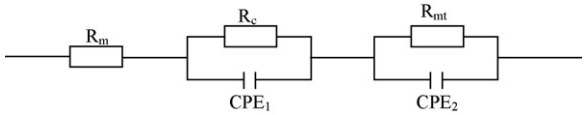

Fig. 6. Equivalent circuit for AC impedance data fitting. R_m: membrane resistance; R_c: kinetic resistance; R_{mt}: mass transfer resistance; CPE_1 and CPE_2: constant phase elements connected in parallel with kinetic and mass transfer resistances, respectively.

catalyst layer and the GDL; and CPE_2 represents the R_{mt} associated capacitance.

Fig. 7 illustrates the contributions of individual resistance gain to the total resistance gain caused by toluene contamination, as a function of toluene concentration at different-current densities. The individual resistance gain, dR_i, is defined as the difference between the fitted individual resistance in the presence of toluene and that in the absence of toluene, and the total resistance gain, ΣdR_i, is estimated by the sum of the three individual resistance gains,

$$dR_i = R_{i,\text{contamination}} - R_{i,\text{baseline}} \quad (4)$$

where i = membrane, kinetic, or mass transfer:

$$\sum dR_i = dR_m + dR_c + dR_{mt} \quad (5)$$

In Fig. 7, the coloured bars represent the relative resistance gains of individual resistances (membrane, kinetic, and mass transfer) in percentage units. Due to errors associated with the measurement and numerical fitting of the resistances, in some instances the relative resistance gains are negative in Fig. 7. Taking those errors into consideration, it is concluded that: (1) membrane resistance is not affected by the presence of toluene in the air stream at all toluene concentrations and current densities; (2) both the kinetic and mass transfer resistances increase due to toluene contamina-

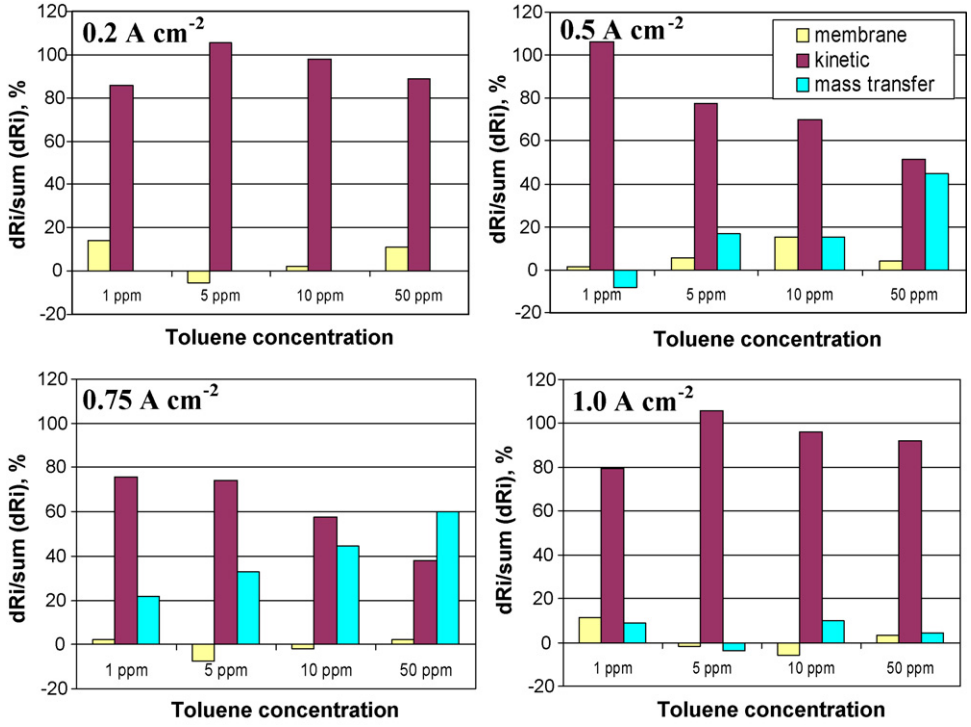

Fig. 7. Contributions of individual resistance increases relative to the total resistance increase at different-current densities, for toluene contamination as tested. Operating conditions: stoichiometry: 1.5/3.0 for H_2/air; RH: 80%; cell temperature: 80 °C; backpressure: 30 psig. MEA: anode/cathode Pt loading: 0.4 mg cm^{-2}.

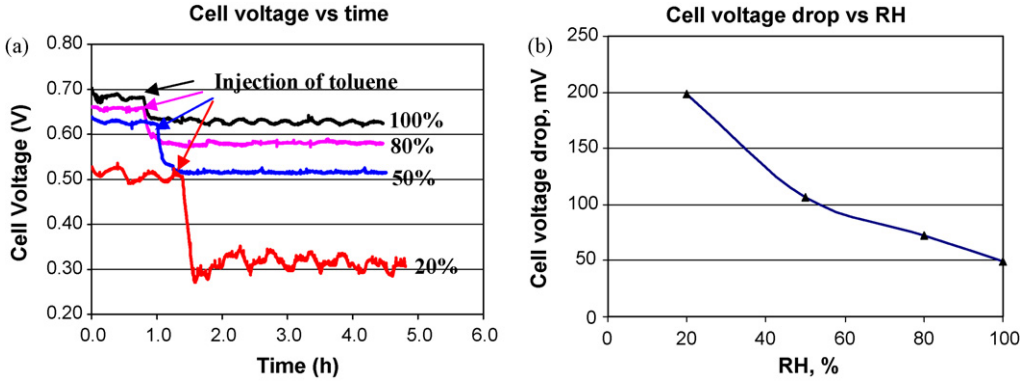

Fig. 8. (a) Contamination tests at various RHs. (b) Cell voltage drops caused by toluene contamination at various RHs. Operating conditions: stoichiometry: 1.5/3.0 for H_2/air; current density: 1.0 A cm^{-2}; cell temperature: 80 °C; backpressure: 30 psig. MEA: anode/cathode Pt loading: 0.4 mg cm^{-2}.

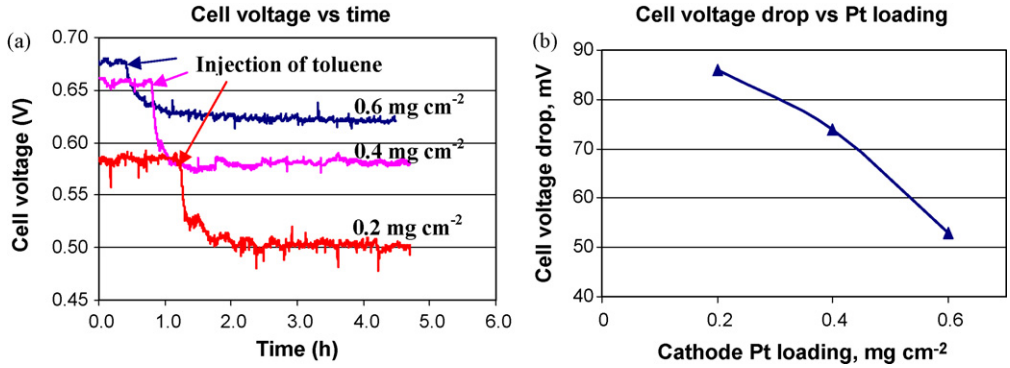

Fig. 9. (a) Contamination tests at various cathode Pt loadings. (b) Cell voltage drops caused by toluene contamination at various cathode Pt loadings. Operating conditions: stoichiometry: 1.5/3.0 for H_2/air; current density: 1.0 A cm^{-2}; cell temperature: 80 °C; backpressure: 30 psig. Anode Pt loading: 0.4 mg cm^{-2}.

tion, but the increase in kinetic resistance is more attributable to cell performance degradation than is the increase in mass transfer resistance, under almost all the tested toluene concentrations and current densities. This suggests that toluene primarily poisons the catalyst layer, causing kinetic loss.

3.2. Effect of RHs

Fig. 8(a) illustrates the results of the contamination tests at four different RHs with 5 ppm toluene, under the operating conditions listed in Table 1, and Fig. 8(b) summarizes the cell voltage drops caused by toluene contamination at different RHs.

As can be seen from Fig. 8(a), cell performance follows the same pattern at all RHs during the contamination test—cell voltage experiences an immediate decline with the introduction of toluene and then reaches a plateau. Fig. 8(b) shows that the cell voltage drop caused by toluene contamination decreases with increasing RH. In other words, the effect of toluene contamination becomes less severe as the RH increases. Two factors could be responsible for this observation. Firstly, as RH increases, the partial pressure of toluene decreases, which could lessen the contamination effect. Secondly, water coverage on the surface of the CCM and/or GDL becomes higher as RH increases, which might wash away some of the adsorbed toluene or prohibit its adsorption, resulting in a less severe contamination effect.

3.3. Effect of cathode Pt loading

The contamination testing results for different cathode Pt loadings are presented in Fig. 9(a), and the cell voltage drop as a function of cathode Pt loading is summarized in Fig. 9(b). As cathode Pt loading increases, the baseline performance increases, but the cell voltage drop caused by toluene contamination decreases, indicating that higher cathode Pt loading makes the MEA less susceptible to toluene contamination.

3.4. Recovery tests

Recovery tests of the toluene-poisoned cell were performed by shutting off the toluene-contaminated air and running the fuel cell with pure air. Fig. 10 shows the results of the recovery test after the fuel cell had been contaminated with 5 ppm toluene at 1.0 A cm^{-2} for about 5 h; a baseline performance without toluene contamina-

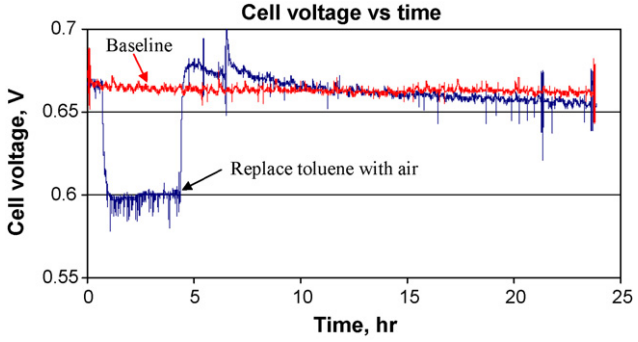

Fig. 10. Recovery test in comparison with baseline. Operating conditions: toluene concentration: 0 ppm for baseline and 5 ppm for the contamination test; current density: 1.0 A cm^{-2}; stoichiometry: 1.5/3.0 for H_2/air; RH: 80%; cell temperature: 80 °C; backpressure: 30 psig. MEA: anode/cathode Pt loading: 0.4 mg cm^{-2}.

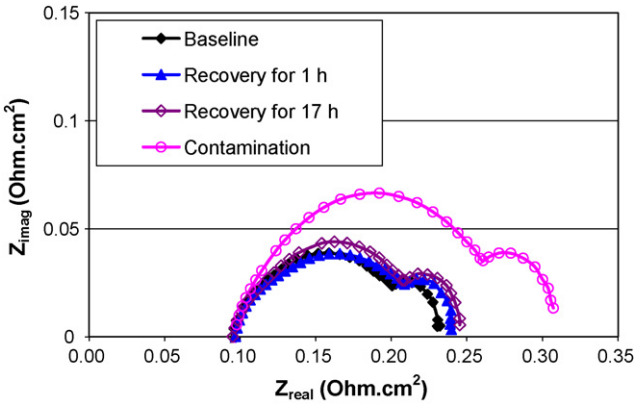

Fig. 11. Nyquist plots at the end of contamination and during recovery. Operating conditions: toluene concentration: 5 ppm; current density: 1.0 A cm^{-2}; stoichiometry: 1.5/3.0 for H_2/air; RH: 80%; cell temperature: 80 °C; backpressure: 30 psig. MEA: anode/cathode Pt loading: 0.4 mg cm^{-2}.

tion, under the same conditions, is given for comparison. As can be seen in Fig. 10, the cell voltage of the toluene-poisoned fuel cell experienced a quick initial recovery to a value that was higher than the baseline cell voltage, but then began to decline. It is not clear why the cell voltage experienced this rapid initial recovery to a value higher than the baseline cell voltage, but the pattern of a quick initial recovery followed by a slow cell voltage decline was observed for all the recovery tests. The decreasing trend of the cell voltage as a result of toluene contamination, in contrast to the constant trend of the baseline performance, suggests that toluene contamination was not fully recoverable because the recovered performance would gradually decline to a voltage level below that of the baseline.

Fig. 11 shows the Nyquist plots obtained at the baseline, at the end of contamination and during recovery. Consistent with the observation explained above regarding cell voltage, the cell resistance – primarily the kinetic resistance (the first semicircle) – increased gradually as the recovery process proceeded.

3.5. Discussion of the contamination mechanisms of toluene

Based upon our toluene contamination testing results in the PEM fuel cell, and upon electrochemical studies of toluene adsorption on a solid Pt electrode [18], it is proposed that toluene degrades cell performance primarily through the kinetic effect and secondarily through the mass transfer effect.

3.5.1. Kinetic effect

It was reported [18,21] that toluene has a strong affinity towards the Pt surface, where it adsorbs through both vertical (σ-complex) and flat (π-complex) orientations that are dependent on temperature and toluene concentration. The adsorption of toluene on the Pt surface has an adverse effect on the ORR activity, and this effect is strongly dependent on both the initial adsorption state of the toluene and the electrode potential. In general, the adsorption of toluene can increase the overpotential of the ORR by blocking Pt active sites, thus degrading the fuel cell performance. The adsorption of toluene can be expressed by the following reaction:

$$C_7H_8 + nPt \rightarrow Pt_n(C_7H_8)_{ads}\,(\sigma\text{-complex and/or }\pi\text{-complex}) \quad \text{(i)}$$

Under PEM fuel cell operating conditions with excess oxygen, the adsorbed toluene may experience deep chemical oxidation to produce CO_2 [21], thus releasing some of the Pt sites for the ORR, as shown in reaction (ii):

$$Pt_n(C_7H_8)_{ads} + 9O_2 \rightarrow 7CO_2 + 4H_2O + nPt \quad \text{(ii)}$$

in which the O_2 can be either free or adsorbed oxygen.

According to Zhu et al. [15] and our results [18], the adsorbed toluene from reaction (i) can also be partially electrochemically oxidized to (1) higher oxidation state intermediates and (2) CO_2, depending on both the orientation of the adsorbed toluene on the Pt surface, as well as the cathode potential. In the temperature range within which a PEM fuel cell operates (around 80 °C), horizontally adsorbed toluene is more prevalent [18], and the product of the electro-oxidation of toluene is primarily CO_2 (reaction (iii)):

$$Pt_n(C_7H_8)_{ads} + mH_2O \rightarrow 7CO_2 + nH^+ + ne^- \quad \text{(iii)}$$

in which the H_2O can be free or adsorbed at the Pt surface.

The intermediate species resulting from toluene electro-oxidation may have some poisoning effect on the catalyst. But the complete oxidation of adsorbed toluene to CO_2 (reaction (iii)) leaves the toluene-occupied Pt surface free for the ORR, thus easing the contamination effect of toluene.

It should be noted that the onset of toluene electrochemical oxidation is in the potential range of 0.8–1.1 V [18]. This range is of prime importance, as it represents the potential region of the air-cathode in a PEM fuel cell operated at OCV and low current densities. In other words, when the PEM fuel cell is operated at OCV and low current densities, the adsorbed toluene is electrochemically oxidized, thus freeing some of the Pt sites for the ORR and resulting in less severe performance degradation, as compared with operation at high current densities.

3.5.2. Mass transfer effect

An interesting observation about the toluene contamination test is that the presence of toluene in the air stream results in water flooding. As can be seen from Figs. 2 and 10, water flooding, reflected in the negative cell voltage spikes, apparently occurs much more often during the contamination period as compared with the baseline. It is also observable from Fig. 2 that the frequency and magnitude of water flooding are enhanced by an increase in both current density and toluene concentration. Furthermore, recovery from toluene contamination by replacing toluene-contaminated air with pure air does not fully recover the fuel cell from water flooding, as shown in Fig. 10, suggesting that toluene contamination causes a permanent change in the hydrophobicity/hydrophilicity of the GDL and/or CCM. We conducted contact angle measurements with both un-contaminated and toluene-contaminated GDLs and CCMs. It was observed that contamination tests with 5 ppm toluene at 50 A cm^{-2} decreased the contact angles of the GDL and CCM by 12° and 14°, respectively. This observation revealed that toluene contamination rendered both the GDL and the CCM more hydrophilic.

Based on these observations, we tentatively propose that toluene adsorption may change the structure and hydrophobicity of the catalyst layer (CL), the GDL, and the ionomer in both the CL and the GDL, thereby causing mass transfer losses. Firstly, the high-surface-area carbon support materials used to support the Pt catalyst in the PEM fuel cell could act as good adsorption substrates for toluene, just as activated carbon has been widely used in industry for removing VOCs, including toluene [22]. This adsorption could significantly change the surface properties, such as the structure and hydrophobicity/hydrophilicity. Secondly, toluene may dissolve into the PTFE of the GDL, which could roughen the PTFE surface or change its surface structure. However, more research is needed to support our theory, such as ex situ characterization of the

contaminated MEA (membrane, catalyst layer, and GDL as well), electrochemical study of toluene adsorption behaviour on a Pt/C electrode, etc.

4. Conclusions

The effect of toluene in air on PEMFC performance was studied using four concentration levels of toluene under five current densities. Cell performance started to drop immediately after the toluene was introduced into the air stream and then reached a plateau. The magnitude of toluene poisoning was a strong function of toluene concentration and current density. With higher toluene concentration and current density, a higher poisoning rate and a larger steady-state cell voltage drop were observed. The effect of toluene on cell performance was also investigated as a function of RH and cathode Pt loading. It was found that increases in RH and cathode Pt loading led to less severe performance degradation.

EIS measurement was employed as a diagnostic tool during the contamination tests to examine changes in cell resistances, including membrane resistance, kinetic resistance, and mass transfer resistance. It was concluded that toluene contamination resulted in an increase in both kinetic and mass transfer resistances, but increased kinetic resistance was a more dominant contributor to the drop in cell performance.

Recovery of the toluene-contaminated fuel cell was conducted by replacing the toluene-contaminated air with pure air. Despite a quick initial recovery in cell performance immediately after the switch from toluene–air to pure air, the fuel cell then experienced a steady decline in performance, which suggests that toluene contamination is not fully recoverable.

A mechanism of toluene contamination was proposed based on our contamination testing results. Adsorption of toluene on the Pt surface and probably also on the high-surface-area carbon support of the catalyst may occupy the active Pt sites and change the catalyst structure, thus poisoning the catalyst. Moreover, the adsorption of toluene may change the surface structure and hydrophobicity/hydrophilicity of the cathode's GDL and CCL, thus rendering the GDL/CCL more hydrophilic.

Acknowledgments

The authors gratefully acknowledge financial support from the Institute for Fuel Cell Innovation, National Research Council of Canada (NRC-IFCI), Ballard Power Systems Inc., and Hydrogenics Corp.

References

[1] S.M. Park, T.J. O'Brien, Technical Report (#DOE/METC/RI-80/16), Department of Energy, Morgantown, W.V. USA, 1980.
[2] P.R. Hayter, P. Mitchell, R.A.J. Dams, C. Dudfield, N. Gladding, Contract Report (ETSUF/02/00126/REP), Wellman CJB Ltd., Portsmouth, UK, 1997.
[3] X. Cheng, Z. Shi, N. Glass, L. Zhang, J.J. Zhang, D.T. Song, Z.S. Liu, H.J. Wang, J. Shen, J. Power Sources 165 (2007) 739.
[4] N. Rajalakshmi, T.T. Jayanth, K.S. Dhathathreyan, Fuel Cells 3 (2003) 177.
[5] W. Shi, B. Yi, M. Hou, Z. Shao, Int. J. Hydrogen Energy 32 (2007) 4412.
[6] J.J. Baschuk, X.G. Li, Int. J. Energy Res. 25 (2001) 695.
[7] Z. Shi, D.T. Song, J.J. Zhang, Z.S. Liu, S. Knights, R. Vohra, N.Y. Jia, D. Harvey, J. Electrochem. Soc. 154 (7) (2007) B609–B615.
[8] J.J. Zhang, H.J. Wang, D.P. Wilkinson, D.T. Song, J. Shen, Z.S. Liu, J. Power Sources 147 (2005) 58.
[9] S. Knights, N.Y. Jia, C. Chuy, J.J. Zhang, Fuel Cell Seminar Extended Abstracts, Palm Springs, CA, 2005, p. 121.
[10] F. Jing, M. Hou, W. Shi, J. Fu, H. Yu, P. Ming, B. Yi, J. Power Sources 166 (2007) 172.
[11] J.M. Moore, P.L. Adcock, J.B. Lakeman, G.O. Mepsted, J. Power Sources 85 (2000) 254.
[12] D. Yang, J. Ma, L. Xu, M. Wu, H. Wang, Electrochim. Acta 51 (2006) 4039.
[13] R. Mohtadi, W. Lee, J.W. Van Zee, J. Power Sources 138 (2004) 216.
[14] S.J. Stranick, M.M. Kamna, P.S. Weiss, Surf. Sci. 338 (1995) 41.
[15] J. Zhu, T. Hartung, D. Tegtmeyer, H. Baltruschat, J. Heitbaum, J. Electroanal. Chem. 244 (1988) 273.
[16] H. Li, Y.H. Tang, Z.W. Wang, Z. Shi, S.H. Wu, D.T. Song, J.L. Zhang, K. Fatih, J.J. Zhang, H.J. Wang, Z.S. Liu, R. Abouatallah, A. Mazza, J. Power Sources 178 (2008) 103.
[17] K. Teranishi, K. Kawata, S. Tsushima, S. Hirai, Electrochem. Solid-State Lett. 9 (10) (2006) A475–A477.
[18] K. Fatih, Z. Shi, D.T. Song, H. Li, J.L. Zhang, S.H. Wu, H.J. Wang, Z.S. Liu, J.J. Zhang, Langmuir, submitted for publication.
[19] C.J. Song, Y.H. Tang, J.L. Zhang, J.J. Zhang, H.J. Wang, J. Shen, S. McDermid, J. Li, P. Kozak, Electrochim. Acta 52 (2007) 2552–2561.
[20] Y.H. Tang, J.J. Zhang, C.H. Song, H.S. Liu, J.L. Zhang, H.J. Wang, S. Mackinnon, T. Peckham, J. Li, S. Mcdermid, P. Kozak, J. Electrochem. Soc. 153 (2006) A2036–A2043.
[21] A.L. Marsh, D.J. Burnett, D.A. fischer, J.L. Gland, J. Phys. Chem. B 108 (2004) 605–611.
[22] M.A. Lillo-Rodenas, D.C. Amoros, A.L. Solano, Carbon 43 (2005) 1758–1767.